JOURNAL OF COMPUTATIONAL PHYSICS, 37, 218–241 (1980)

Adaptive Estimation Procedures for Multi-Parameter Monte Carlo Computations

DONALD L. HITZL

Lockheed Palo Alto Research Laboratory, Dept. 52–56; Bldg. 580, 3460 Hillview Ave., Palo Alto, California 94304

AND

FREDERICK H. MALTZ

Naval Underwater Systems Center, Code 3211, New London, Connecticut 06320

Received August 14, 1979; revised October 31, 1979

This paper describes further developments of a Monte Carlo variance reduction technique which was originally devised by Chorin in 1971. The basic idea of expanding the estimator using orthonormal Hermite polynomials as basis functions has now been extended by the authors to include: (i) multi-parameters, (ii) symmetrized estimators of increased efficiency, and (iii) an adaptive series selection algorithm so that only those coefficients determined with sufficient precision are retained in the Hermite polynomial expansion of the estimator. The so-called Tri-Symmetric Chorin (TSC) estimator is described in detail and computational results obtained using the adaptive algorithm are presented for 6- and 12-parameter problems.

INTRODUCTION

For multi-parameter problems, Monte Carlo computations are frequently performed in order to obtain a statistically realistic simulation while accepting, as a concomitant restriction, the rather slow convergence of the desired estimates to their true values. As a result, a wide variety of procedures have been developed for reducing the error variance in Monte Carlo calculations.

A particularly simple and straightforward technique was proposed by Chorin [1] in 1971; subsequently this method has been revised and improved by the authors [2, 3]. The principal extensions have been to include multiparameter simulations [2], symmetrized estimators of increased computational efficiency [3], and an adaptive series selection algorithm to refine the generalized Hermite polynomial expansion of the estimator [3 and this paper].

The idea of using stochastic series to achieve variance reduction is not new. An example is the orthonormal function method of Ermakov and Zolotukhin [4, pp. 69–73]. The novelty of the Chorin technique lies in the fact that it is a straightforward, two-step procedure which can be readily implemented on the com-

0021-9991/80/110218–24$02.00/0

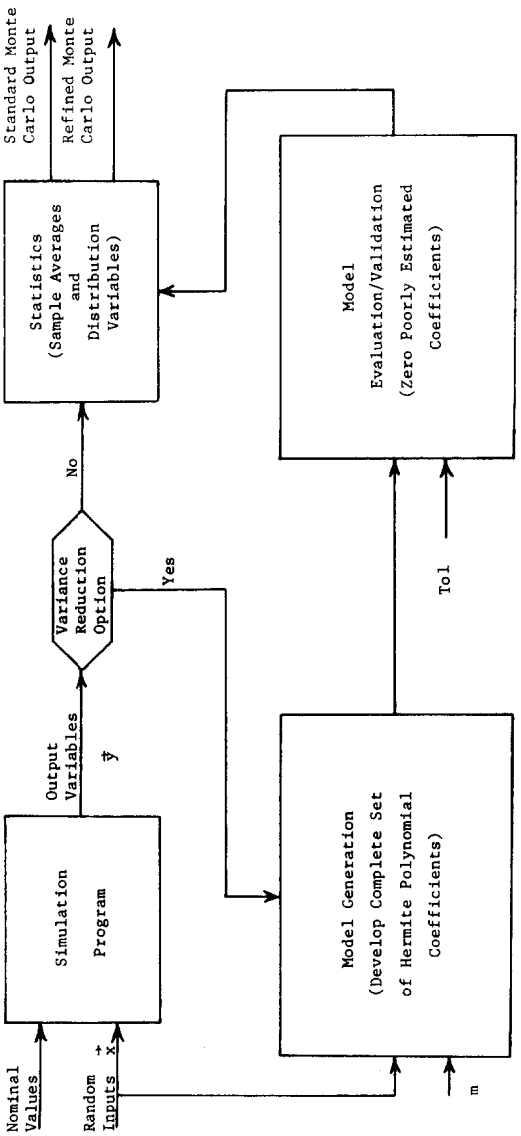

FIG. 1. Data processing procedures for the ordinary and refined Monte Carlo-estimates.

puter. Further, the Chorin-type estimators have desirable convergence properties for large sample sizes and the exact Monte Carlo error variance can be easily evaluated.

The basic approach implemented here to obtain variance reduction is illustrated in Fig. 1. A stochastic error model is generated using the existing data and "tuned" by comparing certain "normalized variance reduction discriminants" with a preset tolerance level. Provided a suitable system model can be identified (which is always the case except for very small data sets and very tight tolerance levels), improved estimates of higher precision can be determined and variance reduction is assured.

This paper is structured as follows. First, the fully symmetrized estimator, or the so-called Tri-Symmetric Chorin (TSC) extension of the basic Chorin (C) estimator, is developed. (The Symmetric Chorin (SC) estimator was derived in [2]). Next, it is shown that the Monte Carlo error variance for the TSC estimator is smaller than that for the C estimator *under all conditions.* Then the adaptive algorithm is described and, finally, computational results are presented for the following two problems:

1. A simplified three-dimensional (3-D) reentry trajectory simulation with six random variables.

2. The Deployment Dispersion Function—a 12-parameter model for the dispersion of coasting trajectories after separation from a post-boost vehicle. This problem was described previously in [2] but results using the symmetrized estimators (SC and TSC) and the adaptive option were not available then.

Now, before closing this section, we would like to reproduce the following quotation from Halton [5, p. 47], as this captures an important aspect of the present work.

> The Monte Carlo method was developed for use on large electronic digital computers, and although it can be applied to pencil and paper calculations, its exponents have always worked close to computers, both in judging the usefulness of their techniques and in developing the theory of their subject. The study of the Monte Carlo method is one of the best examples of the *creative use of computers as a research tool*, and it is to be hoped and expected that future work will be in the same spirit.

The particular relevance of this statement will be discussed in the later section on computational results.

Fully Symmetrized Estimator

The basic Chorin estimator f^* for the unknown function f is given by Eq. (15) in [2] as

$$f^* = \hat{f} - \Delta f_0 = \frac{1}{M} \sum_{i=1}^{M} \left\{ f(\mathbf{x}_i) - \sum_{k=1}^{m} \hat{a}'_k \Phi_k(\mathbf{x}_i) \right\} \tag{1}$$

where

(a) Δf_0 is an estimate of the residual $f - E[f]$,

(b) $f = f(\mathbf{x})$ is a function of a p-dimensional random vector $\mathbf{x}$ all of whose components have mean zero and variance one and are uncorrelated,

(c) $\Phi_k(\mathbf{x})$ is the multi-parameter generalization of the usual orthonormal Hermite polynomials $\Phi_k(x)$ appropriate to a single variable.

Thus, the "corrector series" Δf_0 is a zero-mean Hermite polynomial expansion modeling the stochastic fluctuations in f resulting from the random inputs $\mathbf{x}_i$.

Following the notation in [2], the estimator f^* is obtained by first splitting $N = 2M$ statistically independent samples into two sets,

$$\begin{aligned} S &= \{\mathbf{x}_i, i = 1, 2, \ldots, M\}, \\ S' &= \{\mathbf{x}'_i, i = 1, 2, \ldots, M\}, \end{aligned} \tag{2}$$

and then using the set S' to estimate the coefficients

$$\hat{a}'_k = \frac{1}{M} \sum_{i=1}^{M} f(\mathbf{x}'_i)\, \Phi_k(\mathbf{x}'_i). \tag{3}$$

Next, the set S is used to form the final estimate

$$f^* \triangleq f^*(S, S') \tag{4}$$

given by Eq. (1) above.

In order to make better use of the available samples, it was found by the authors [2, 3] that the Chorin estimator could be symmetrized. By reversing the roles of the sample sets S and S' and repeating the previous two-step procedure, two Chorin estimators

$$\begin{aligned} f_1^* &= f^*(S, S'), \\ f_2^* &= f^*(S', S) \end{aligned} \tag{5}$$

are obtained. Their average then yields the symmetric Chorin (SC) estimate

$$f_{SC}^* = \tfrac{1}{2}(f_1^* + f_2^*), \tag{6}$$

which, as shown in Eqs. (26) and (34) of [2], has an asymptotic (large N) error variance equal to $\frac{1}{2}$ that of the basic Chorin estimator.

Even further improvements can be realized, however, by partitioning all N Monte Carlo samples into three statistically independent sets of M samples each ($N = 3M$). Thus, we append

$$S'' = \{\mathbf{x}''_i, i = 1, 2, \ldots, M\} \tag{7}$$

to S and S' given by Eq. (2) and form the three Chorin estimates

$$\begin{aligned} f_1^* &= f^*(S, S'), \\ f_2^* &= f^*(S', S''), \\ f_3^* &= f^*(S'', S). \end{aligned} \tag{8}$$

Their average then defines the fully symmetrized, or tri-symmetric, Chorin estimate

$$f_{\mathrm{TSC}}^* = \tfrac{1}{2}(f_1^* + f_2^* + f_3^*). \tag{9}$$

Now, one of the main purposes of this section is to show that the three estimates f_i^* in Eq. (8) are mutually uncorrelated so that, in contrast to the error variance for the SC estimate derived in [2], the exact error variance for the TSC estimator has no additional penalty term.

The error variance for the TSC estimate is

$$\sigma_{\mathrm{TSC}}^2 = \tfrac{1}{3}\sigma_{\mathrm{C}_i}^2 + \tfrac{2}{9}(\mathrm{Cov}[f_1^*, f_2^*] + \mathrm{Cov}[f_1^*, f_3^*] + \mathrm{Cov}[f_2^*, f_3^*]), \tag{10}$$

where $\sigma_{\mathrm{C}_i}^2$ is the basic Chorin error variance given by Eq. (20) in [2] as

$$\sigma_{\mathrm{C}_i}^2 = \frac{A}{M_i} + \frac{B}{M_i^2} = \frac{2A}{N_i} + \frac{4B}{N_i^2} \tag{11}$$

for any of the three individual Chorin estimates in (9). Note that the individual Chorin estimates each use a total of N_i samples with $M_i = \frac{1}{2}N_i = \frac{1}{3}N$. From the structure of the estimates given in (8),

$$\mathrm{Cov}[f_1^*, f_2^*] = \mathrm{Cov}[f_2^*, f_3^*] \tag{12}$$

so

$$\sigma_{\mathrm{TSC}}^2 = \tfrac{1}{3}\sigma_{\mathrm{C}_i}^2 + \tfrac{4}{9}\,\mathrm{Cov}[f_1^*, f_2^*] + \tfrac{2}{9}\,\mathrm{Cov}[f_1^*, f_3^*]. \tag{13}$$

Now, applying Eq. (1) three times, we have

$$\begin{aligned} f_1^* &= \hat{f} - \hat{\Delta f}_0, \\ f_2^* &= \hat{f}' - \hat{\Delta f}_0', \\ f_3^* &= \hat{f}'' - \hat{\Delta f}_0'', \end{aligned} \tag{14}$$

with

$$\begin{aligned} \hat{\Delta f}_0 &\triangleq \sum_1^m \hat{a}_i' \hat{\boldsymbol{\Phi}}_i(\mathbf{x}), \\ \hat{\Delta f}_0' &\triangleq \sum_1^m \hat{a}_j'' \hat{\boldsymbol{\Phi}}_j(\mathbf{x}'), \\ \hat{\Delta f}_0'' &\triangleq \sum_1^m \hat{a}_k \hat{\boldsymbol{\Phi}}_k(\mathbf{x}''). \end{aligned} \tag{15}$$

Referring to Eq. (3), the individual coefficients are estimated as

$$\begin{aligned} \hat{a}_i' &= \widehat{f(\mathbf{x}')\,\Phi_i(\mathbf{x}')}, \\ \hat{a}_j'' &= \widehat{f(\mathbf{x}'')\,\Phi_j(\mathbf{x}'')}, \\ \hat{a}_k &= \widehat{f(\mathbf{x})\,\Phi_k(\mathbf{x})}. \end{aligned} \tag{16}$$

With these preliminaries, we first show

$$\mathrm{Cov}[f_1^*, f_2^*] = E[\hat{\Delta f}_0\,\hat{\Delta f}_0'] \tag{17}$$

by applying the definition

$$\mathrm{Cov}[f_1^*, f_2^*] = E[f_1^* f_2^*] - (E[f])^2 \tag{18}$$

and expanding the first term in (18), using (14), to get

$$E[f_1^* f_2^*] = (E[f])^2 - E[\hat{f}\,\hat{\Delta f}_0'] - E[\hat{f}'\,\hat{\Delta f}_0] + E[\hat{\Delta f}_0\,\hat{\Delta f}_0'], \tag{19}$$

where we note that

$$E[\hat{f}\hat{f}'] = E[\hat{f}]\,E[\hat{f}'] = (E[f])^2 \tag{20}$$

since the basic Chorin estimator f^* is unbiased. Next, using Eqs. (15) and (16), we obtain

$$E[\hat{f}\,\hat{\Delta f}_0'] = \sum_1^m E[\hat{f}]\,E[\widehat{f\Phi_j}]\,E[\hat{\Phi}_j'] = 0 \tag{21}$$

and

$$E[\hat{f}'\,\hat{\Delta f}_0] = \sum_1^m E[\hat{f}'\hat{a}_i']\,E[\hat{\Phi}_i] = 0 \tag{22}$$

since $E[\hat{\Phi}_k] = 0$. Thus, the cross terms in Eq. (19) are zero and the desired result (17) follows from (18), (19), and (20).

In exactly the same way, we obtain

$$\mathrm{Cov}[f_1^*, f_3^*] = E[\hat{\Delta f}_0\,\hat{\Delta f}_0'']. \tag{23}$$

Then, using Eqs. (15) once again, we find

$$\mathrm{Cov}[f_1^*, f_2^*] = \sum_1^m \sum_1^m E[\hat{a}_i'\hat{\Phi}_j']\,E[\hat{a}_j'']\,E[\hat{\Phi}_i] = 0 \tag{24}$$

and

$$\mathrm{Cov}[f_1^*, f_3^*] = \sum_1^m \sum_1^m E[\hat{a}_i']\,E[\hat{a}_k\hat{\Phi}_i]\,E[\hat{\Phi}_k''] = 0 \tag{25}$$

so that, finally, Eq. (10) becomes

$$\sigma^2_{\mathrm{TSC}} = \frac{1}{3}\sigma^2_{\mathrm{C}_i} = \frac{A}{3M_i} + \frac{3B}{9M_i^2} = \frac{A}{N} + \frac{3B}{N^2} < \frac{2A}{N} + \frac{4B}{N^2} \equiv \sigma^2_{\mathrm{C}}. \tag{26}$$

Consequently, for all A, B, and N, the Monte Carlo error variance for the TSC estimator σ^2_{TSC} is indeed smaller than that for the basic Chorin estimator.

Adaptive Algorithm

In order to obtain the best possible results in Monte Carlo simulations using these advanced estimators, it is most important to assess which terms in the corrector series Δf_0 given in Eq. (1) yield a net variance decrease. This is especially true if the dimensionality p is somewhat high, so that the Hermite series becomes rather large. In fact, it should be noted that the upper limit m for the orthonormal expansion of Δf_0 in Eq. (1) is actually of the form $m(m, p)$, where

m = highest order polynomial to be retained,

p = number of parameters,

so

$$m(m, p) = \frac{(m+p)!}{m!\,p!}. \tag{27}$$

For example, if $m = 3$ (so we include linear, quadratic, and cubic terms) and $p = 10$, $m(3, 10) = 286$.

The method we use for selecting which terms in Δf_0 are important is referred to as the adaptive series selection algorithm. The label "adaptive" is used because the corrector series is automatically "tailored" for each value of N used in the computations. This algorithm will be described here for the fully symmetrized TSC estimator but it has also been implemented for the other estimators C and SC.

The Monte Carlo error variance σ^2_{TSC} for the tri-symmetric Chorin estimator is given by Eq. (26),

$$\sigma^2_{\mathrm{TSC}} = \frac{A}{N} + \frac{3B}{N^2}, \tag{26}$$

where A is the mean square remainder in the truncated Hermite series expansion

$$A = \sum_{m+1}^{\infty} a_k^2 = \sigma^2 - \sum_{1}^{m} a_k^2 \tag{28}$$

and B is the sum of the error variances for the coefficient estimates $\hat{a}_k$,

$$B = \sum_{1}^{\infty} b_k^2 \qquad \text{with} \quad b_k^2 = \text{Var}[f\Phi_k] = \text{Var}[a_k]. \tag{29}$$

Inserting (28) and (29) into (26)

$$\sigma_{\text{TSC}}^2 = \frac{1}{N}\left[\sigma^2 - \sum_{1}^{m}\left(a_k^2 - \frac{1}{M}b_k^2\right)\right] \tag{30}$$

since $N = 3M$. Using Eq. (30), we then define

$$\Delta_k \triangleq a_k^2 - \frac{1}{M}b_k^2, \tag{31}$$

where we see immediately that variance reduction occurs for the kth term provided $\Delta_k > 0$. Thus, since the effect of individual terms can now be assessed, we refer to the quantity Δ_k as the *variance reduction discriminant.* Finally, since both terms in Eq. (31) are positive, it has proven more convenient to consider instead

$$\bar{\Delta}_k \triangleq \frac{M^{-1}b_k^2}{a_k^2}, \tag{32}$$

where, for variance reduction, $\bar{\Delta}_k < 1$. This quantity $\bar{\Delta}_k$ is termed the *normalized variance reduction discriminant.*

Now, since a_k^2 is the variance of the component $a_k\Phi_k(\mathbf{x})$ in the polynomial expansion of f and $(1/M)b_k^2$ is the error variance for the M-sample estimate of the coefficient a_k, we see that $\bar{\Delta}_k$ can be considered as representing the inverse signal to noise ratio squared $(S/N)^{-2}$ so we define the adaptive series selection criteria (Tolerance) as

$$\text{Tol} = (S/N)^{-2} \tag{33}$$

and require

$$\bar{\Delta}_k < \text{Tol} \leqslant 1. \tag{34}$$

This is the basis of the adaptive multi-parameter simulation results to be presented in the next section.

Computational Results

Simulation results using two model problems are presented now. The first is a simplified three-dimensional (3-D) reentry trajectory simulation with six random variables. This is an essential simplification of the full 6-D reentry trajectory simula-

tion [6] since the attitude motion of the spinning vehicle has now been removed and only a restricted 3-D computation giving the longitudinal (in plane) and lateral (out of plane) motions of the mass center has been retained. Also, the full simulation contains 32 random inputs while this reduced problem includes only the following six random input parameters:

$p_1 = \Delta C_A$ = change in axial force coefficient due to nose shape change resulting from ablation,

$p_2 = \phi$ = roll orientation of ΔV $(= p_6)$ relative to the nominal trajectory plane $(0 \leqslant \phi \leqslant 2\pi)$,

$p_3 = W$ = initial reentry vehicle weight,

$p_4 = \Delta C_{A_{SF}}$ = change in skin friction coefficient,

$p_5 = \Delta W$ = weight loss during reentry,

$p_6 = \Delta V$ = net lateral velocity increment resulting from boundary layer transition (laminar to turbulent flow).

TABLE I

Number of Terms Retained in Hermite Series Using Adaptive Series Selection Algorithm

						Number of terms		
m	$m(m,p)$[a]		Quantity	N	Tol	SC	TSC	Figure No.
			Reentry Simulation with $p = 6$					
1	7		DR	198	$\frac{1}{2}$	3	3	3a, b
1	7		CR	198	$\frac{1}{2}$	3	2	5a, b
2	28		DR	198	$\frac{1}{4}$	4	3	4a, b
2	28		DR	198	$\frac{1}{2}$	6	7	—[b]
2	28		CR	198	$\frac{1}{2}$	6	4	—
			Deployment Simulation with $p = 12$					
2	91	(11)[c]	y_3	600	$\frac{1}{16}$	8	6	6a, b
2	91		y_1^2	240	$\frac{1}{4}$	8	6	—
2	91		y_1^2	360	$\frac{1}{4}$	9	8	—
2	91		y_1^2	480	$\frac{1}{4}$	11	10	—
2	91	(11)	y_1^2	600	$\frac{1}{4}$	11	11	7a, b
2	91	(63)	$y_2 y_3$	600	$\frac{1}{2}$	43	37	8a, b

[a] $m(m,p)$ = total number of terms in Hermite series $= (m+p)!/m!\,p!$.

[b] Plots not included.

[c] Exact number of terms for full correction.

The principal objective of this simulation was then to assess the downrange and crossrange dispersions of the nominal impact point due to the combined (and coupled) effects of random perturbations in the previous six dominant error sources.

Results for the normalized variance reduction discriminants $\bar{\Delta}_k$ are shown first in Figs. 2a and 2b for the SC and TSC estimators, respectively. These plots have been included here principally so that the following chronology can be described. Initially, it was desired to plot $\Delta_1, \Delta_2, \ldots$ versus N but it was found that the individual Δ_k varied

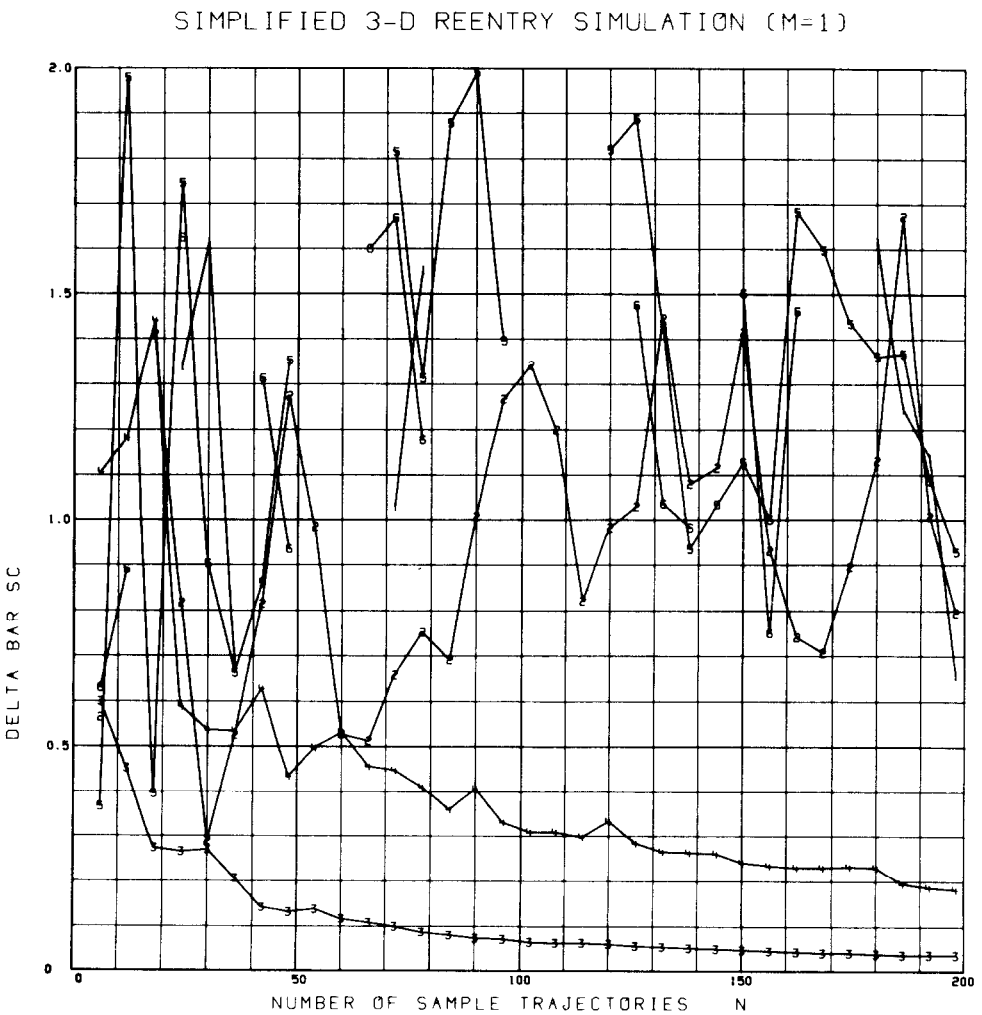

FIG. 2a. Normalized variance reduction discriminants $\bar{\Delta}_k$ ($k = 1, 2, \ldots, 6$) for the SC estimate as a function of the number of trajectories N. Note that only the linear coefficients for parameters 3 and 4 are consistently estimated with sufficient precision ($\bar{\Delta}_k < 1$) for use in the stochastic corrector series.

over several orders of magnitude. Hence, we were led to the idea of normalizing and Figs. 2a, 2b were obtained where we see vividly that only two parameters are fitted consistently in the linear corrector series. This then led to the *concept* of the adaptive tolerance level described in the previous section. And this sequence of events, we submit, is *exactly* in the spirit of the comment by Halton quoted in the Introduction.

Simulation results are presented next in Figs. 3a to 4b for the downrange impact point and in Figs. 5a, b for the crossrange impact point. In each case, estimates of the mean are presented in the "a" figure while the corresponding Monte Carlo error

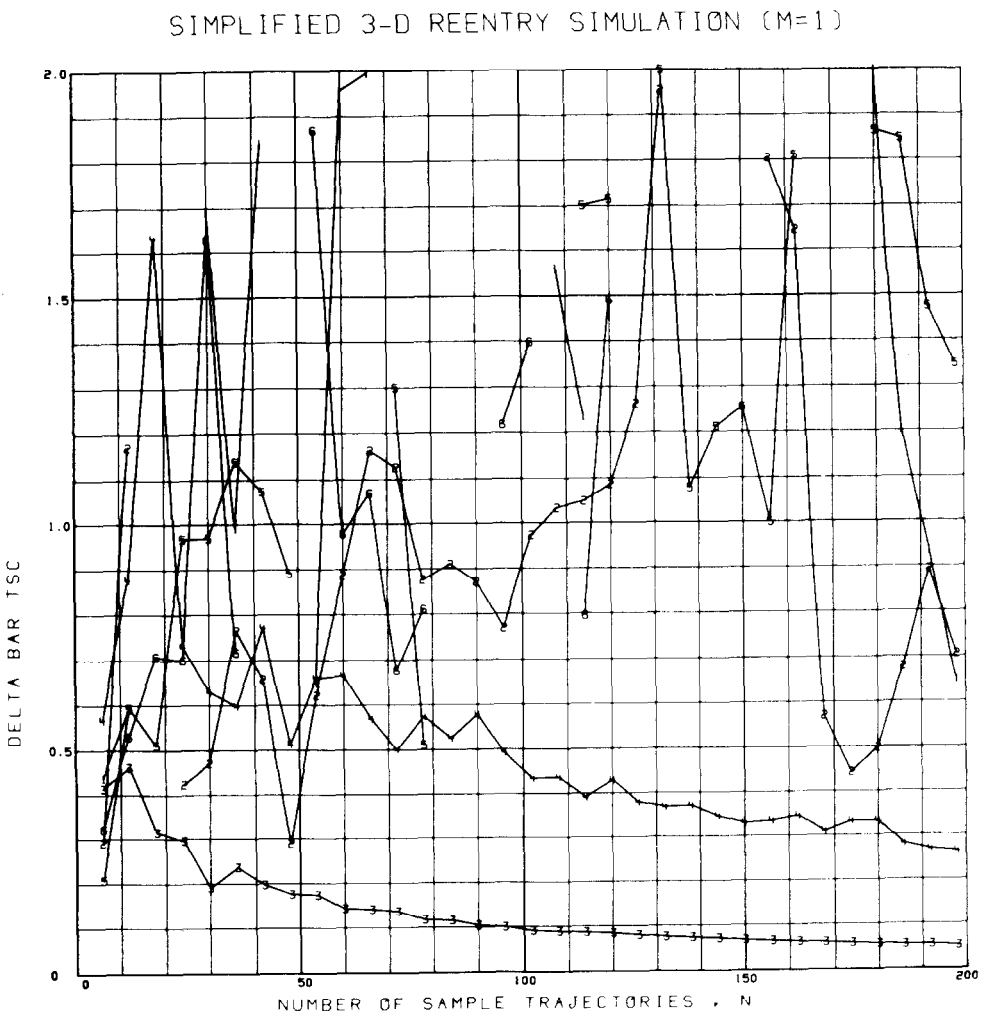

FIG. 2b. Normalized variance reduction discriminants $\bar{\Delta}_k$ $(k = 1, 2, \ldots, 6)$ for the TSC estimate as a function of N. Again, only parameters 3 and 4 are retained in the linear corrector series.

variances are given in the "b" figure. These latter figures can be interpreted in either of two ways. For a given N, the reduction in variance is immediately available while, for a given variance, the allowable reduction in sample size N is easily assessed.

For all the figures presented in this paper, Table I summarizes the performance of the adaptive algorithm for various m, Tol, and N. In general, retaining fewer terms by

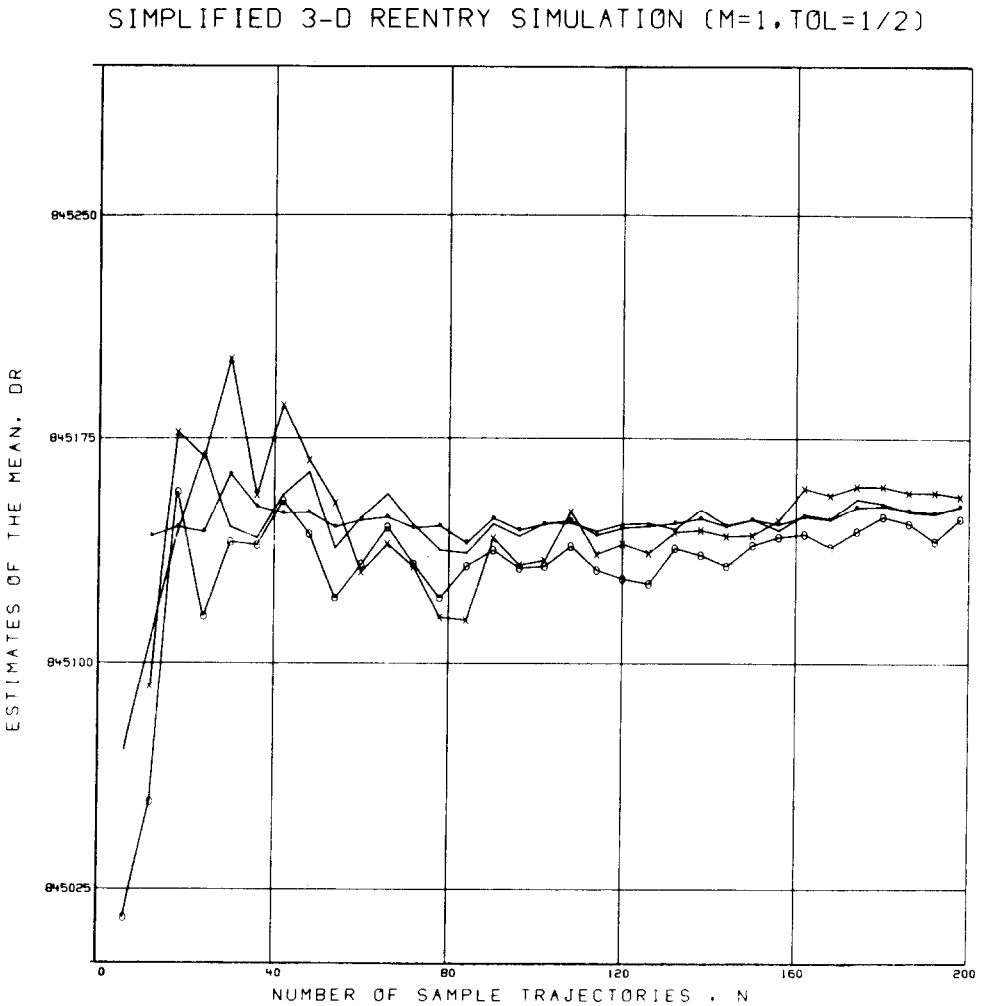

FIG. 3a. Estimates of the mean downrange impact position as a function of N for all four estimators. Here, as in all the plots to follow, the symbols represent: ○—Direct Estimate D, ×—Chorin Estimate C, ∗—Symmetrized Chorin Estimate SC, ·—Tri-Symmetrized Chorin Estimate TSC. These results were obtained with a linear corrector series of six terms and with the adaptive tolerance set equal to $\frac{1}{2}$.

tightening the tolerance leads to decreased variance reduction together with somewhat "smoother" estimates of the mean for low values of N. Alternatively, loosening Tol to values near 1 can give, in some cases, negative Monte Carlo error variances [7] as a result of subtracting too many coefficients in Eq. (28). Thus, there is a necessary interaction between the analyst and the computer when choosing appropriate values for m and Tol. This is accomplished, most effectively, from an interactive terminal.

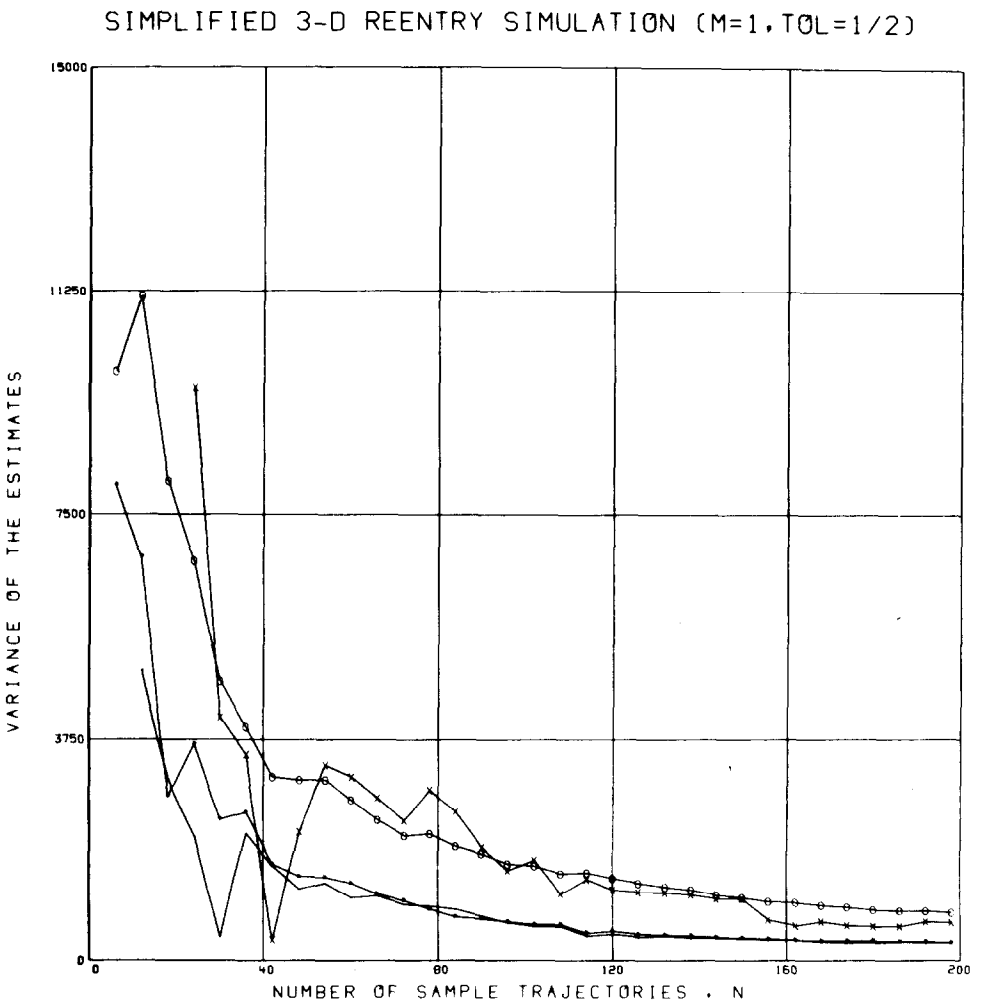

FIG. 3b. Variances for the four estimates shown in Fig. 3a. Note the superior performance (variance reduction) obtained with the two symmetrized estimators, SC and TSC, compared to the original Chorin estimator C.

The appropriate stochastic system models for the 3-D reentry simulation have been identified during these computations as

$$\mathrm{DR} = 845150 + 307.49W - 101.93\Delta C_{A_{SF}} + 159.82\left(\frac{\Delta C_A^2 - 1}{2^{1/2}}\right) + 100.33\left(\frac{\phi^2 - 1}{2^{1/2}}\right) - 48.49\Delta C_A\,\Delta W + 2.239(\phi\,\Delta W), \tag{35}$$

$$\mathrm{CR} = 0.213 + 33.195\phi - 2.924\Delta C_A W - 5.243\Delta C_A\,\Delta C_{A_{SF}} \tag{36}$$

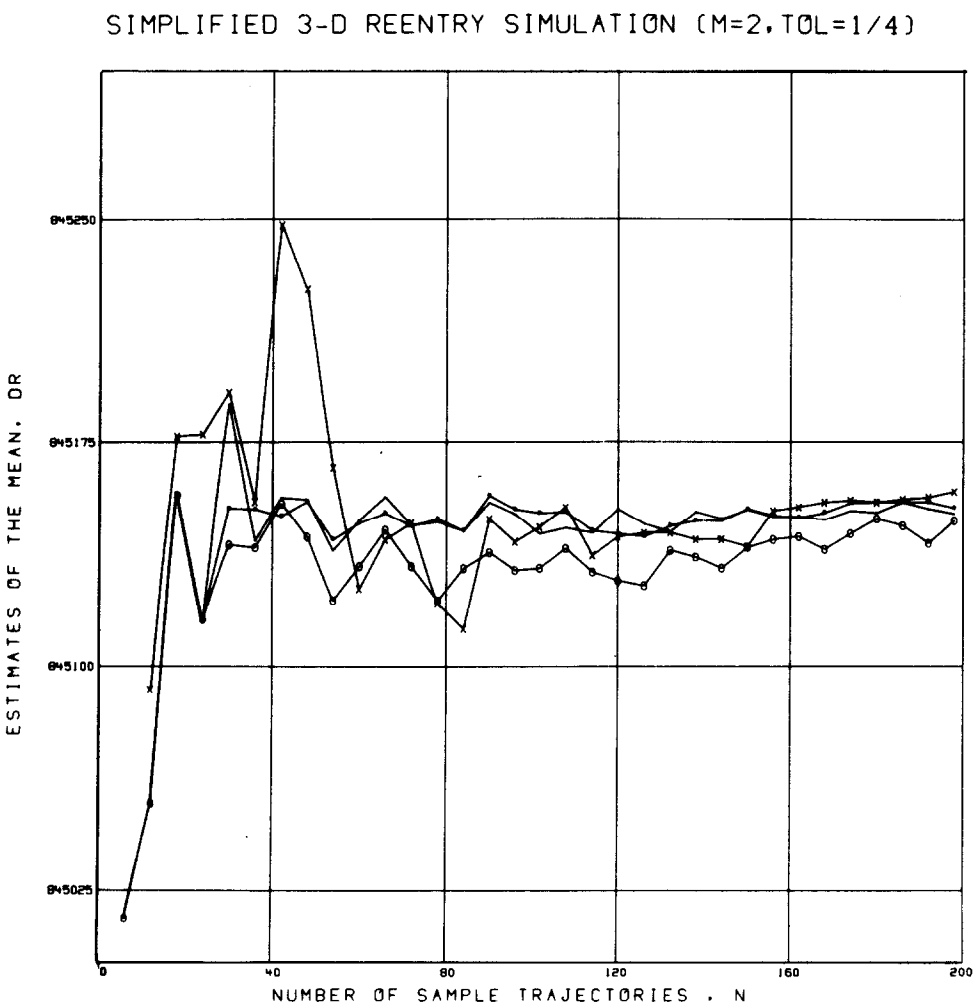

FIG. 4a. Estimates of the mean downrange impact position as a function of N for all four estimators. Now the corrector series contains both linear and quadratic terms (total of 27) and the adaptive threshold has been tightened to $\frac{1}{4}$.

for the TSC estimator using $N = 198$ (all the available sample trajectories), $m = 2$ and $\text{Tol} = \frac{1}{2}$. For comparison, the expressions

$$\text{DR} = 845151 + 307.49W + 159.82\left(\frac{4C_A^2 - 1}{2^{1/2}}\right), \tag{37}$$

$$\text{CR} = 0.450 + 33.195\phi \tag{38}$$

were obtained when the Tolerance was tightened to $\frac{1}{4}$.

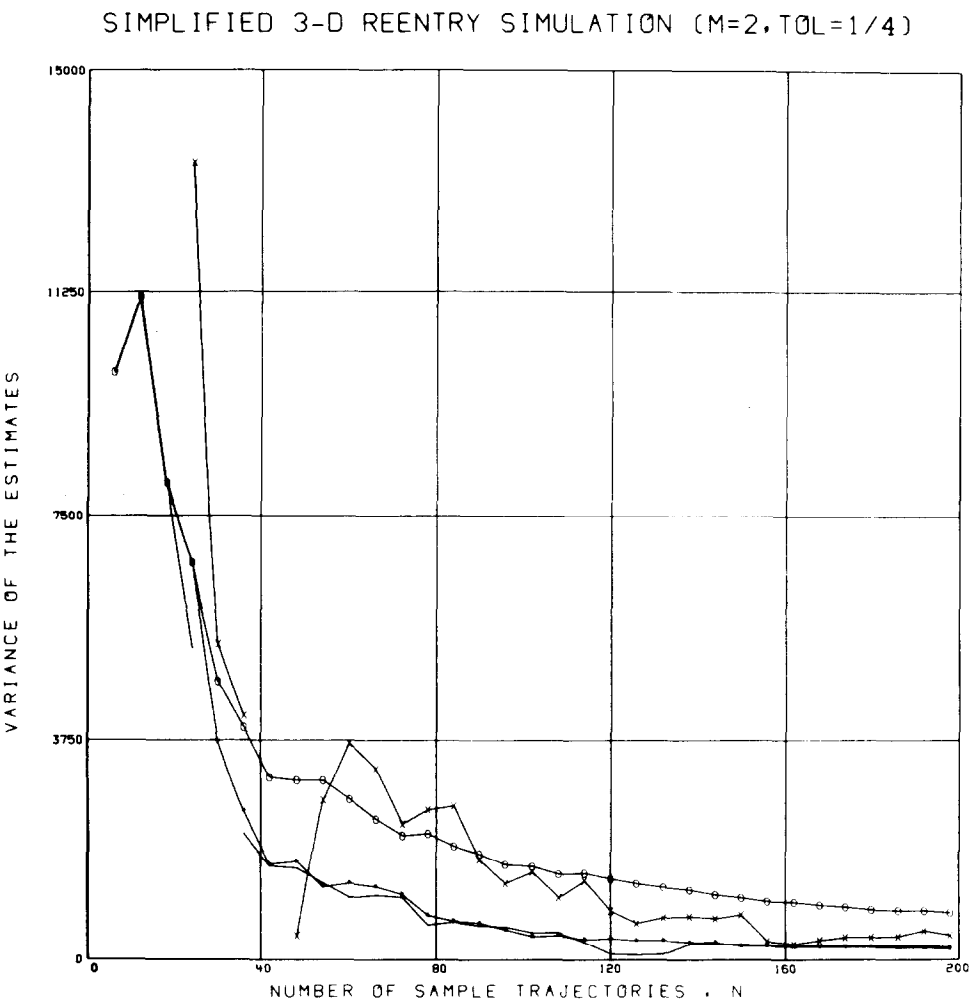

FIG. 4b. Variances for the four estimates shown in Fig. 4a. Comparing to Fig. 3b, we see that further variance reduction has indeed been achieved.

We now proceed to the second model problem—the so-called Deployment Dispersion Function introduced earlier in [2]. The specific example investigated here is

$$\mathbf{y} = A\mathbf{x} + \boldsymbol{\mu}, \tag{39}$$

where $\mathbf{y}^T = [y_1 y_2 y_3]$ is a 3 vector, $\mathbf{x}^T = [x_1 x_2 \cdots x_{12}]$ is a 12 vector whose components have mean zero and variance one and are uncorrelated, $\boldsymbol{\mu}^T = [0\ 3\ 6]$ is a 3 vector of mean values, and A is a (3×12) matrix with integer entries given by Eq. (55) in [2]. For this problem, both the means $E[y_i]$ and second moments $E[y_i^2]$,

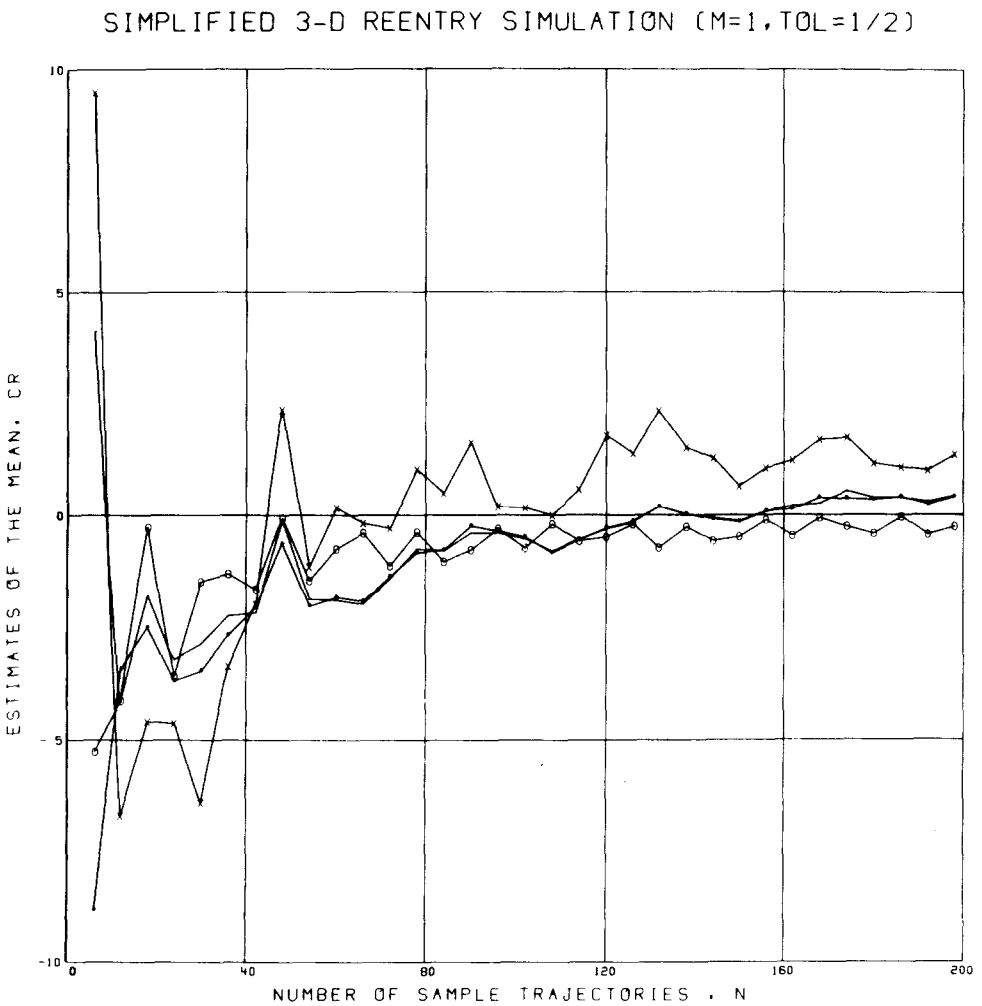

FIG. 5a. Estimates of the mean crossrange impact position as a function of N with a linear corrector series ($m = 1$) and the adaptive threshold $Tol = \frac{1}{2}$.

$E[y_i y_j]$ $\{i = 1, 2, 3;\ j = 1, 2, 3;\ i \neq j\}$ were determined using both the direct (D) and Hermite accelerated Monte Carlo estimators (C, SC, and TSC). However, because of its inferior performance relative to the symmetrized estimators, the basic C estimator was eliminated from the plots given in Figs. 6a to 8b.

Examining these figures, we see that estimates of much higher precision have indeed been obtained. Table I again summarizes the performance of the adaptive algorithm for this problem. Because of the *known* simple structure of this problem, it is quite interesting to investigate the form of the multi-parameter Hermite polynomial expansion determined by the adaptive algorithm during the course of the computation (i.e., as N increases).

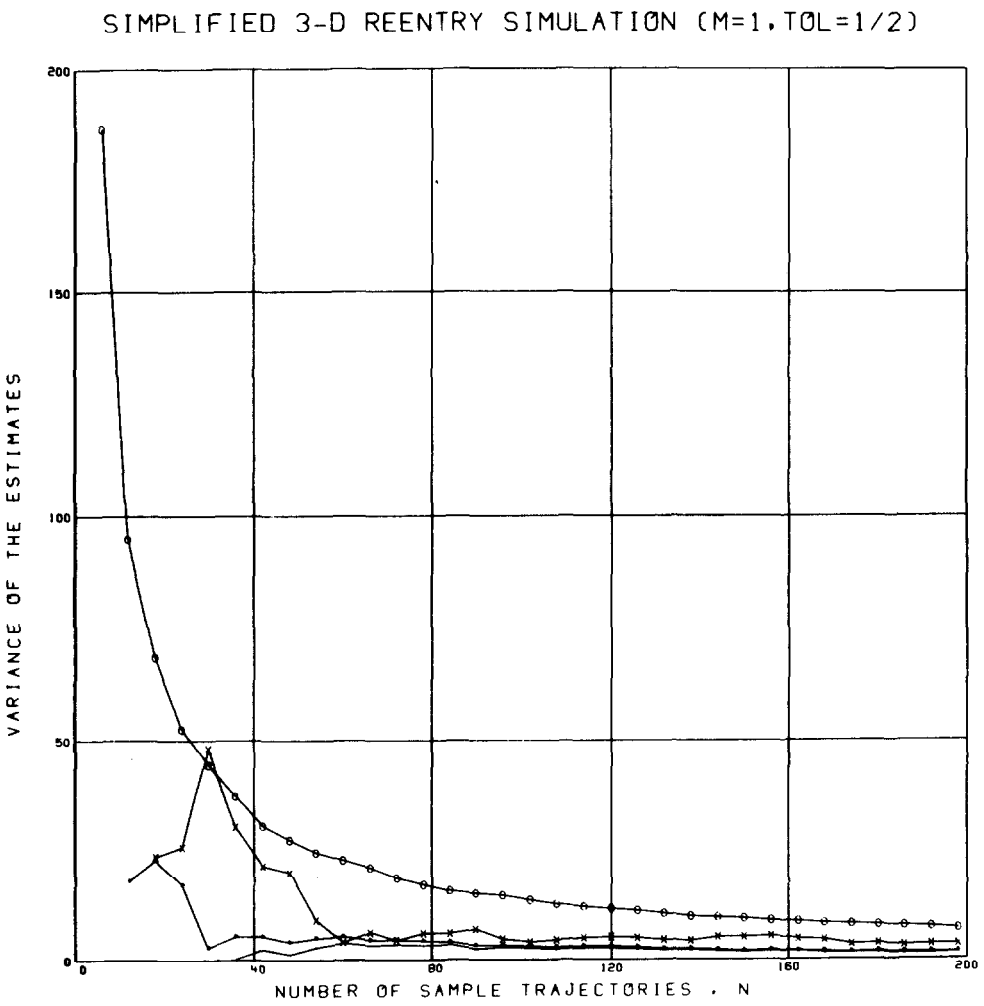

FIG. 5b. Variances for the four estimates shown in Fig. 5a.

For the linear function y_3 shown in Figs. 6a, b, successive determinations of the Hermite series using the TSC estimator with $m = 2$ (intended over correction) and $\text{Tol} = \frac{1}{16}$ (high precision) are

$$\hat{y}_3 = 5.943 + 2.986x_6 + 3.074x_{12} \qquad \text{for} \quad N = 360, \tag{40}$$

$$\hat{y}_3 = 5.981 + 2.951x_3 + 2.905x_6 + 2.892x_9 + 2.862x_{12} \qquad \text{for} \quad N = 480, \tag{41}$$

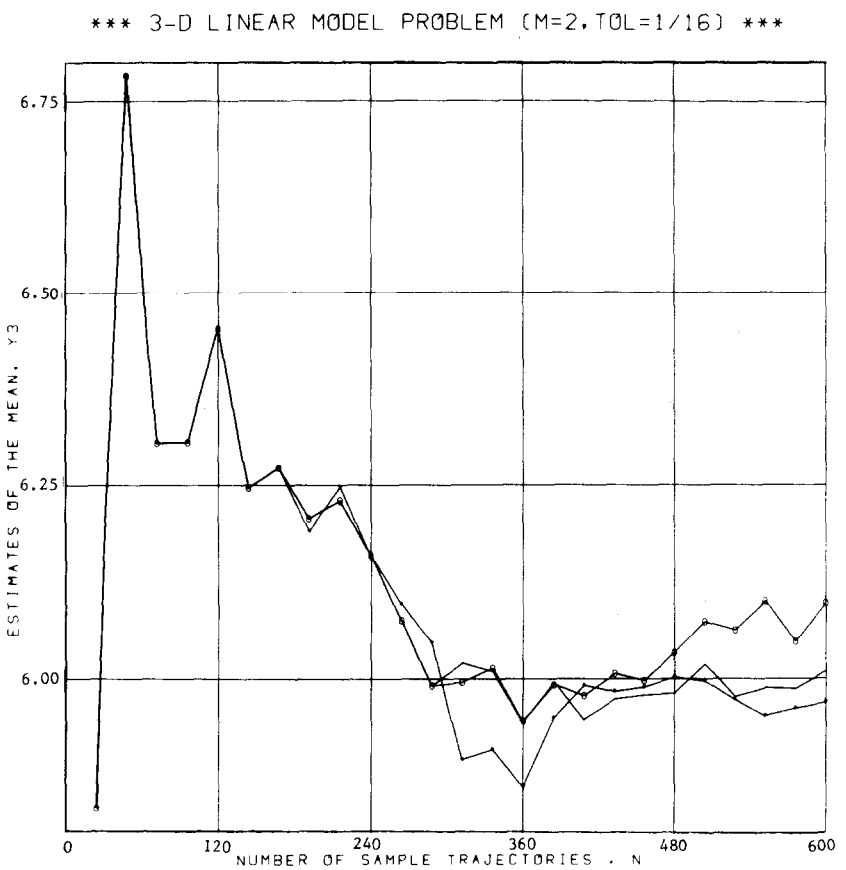

FIG. 6a. Estimates of the mean of y_3 as a function of N for the deployment dispersion function $\mathbf{y} = A\mathbf{x} + \boldsymbol{\mu}$. The exact value is $E[y_3] = 6.0$. The Chorin estimator C has now been dropped for this example problem so only three curves remain. Note that for $N \leqslant 168$, all estimates revert to the ordinary direct estimate D as no terms are retained in the stochastic corrector series while, for $N > 360$, the symmetrized estimators indeed exhibit an acceleration toward convergence.

and

$$\hat{y}_3 = 6.009 + 2.810x_3 + 3.073x_6 + 2.869x_9 + 2.168x_{10} + 2.957x_{12} \quad \text{for} \quad N = 600. \tag{42}$$

These three estimates should be compared with the exact formula

$$y_3 = 6 + x_1 + 2x_2 + 3x_3 + x_5 + 3x_6 + 2x_7 + 3x_9 + 2x_{10} + x_{11} + 3x_{12}. \tag{43}$$

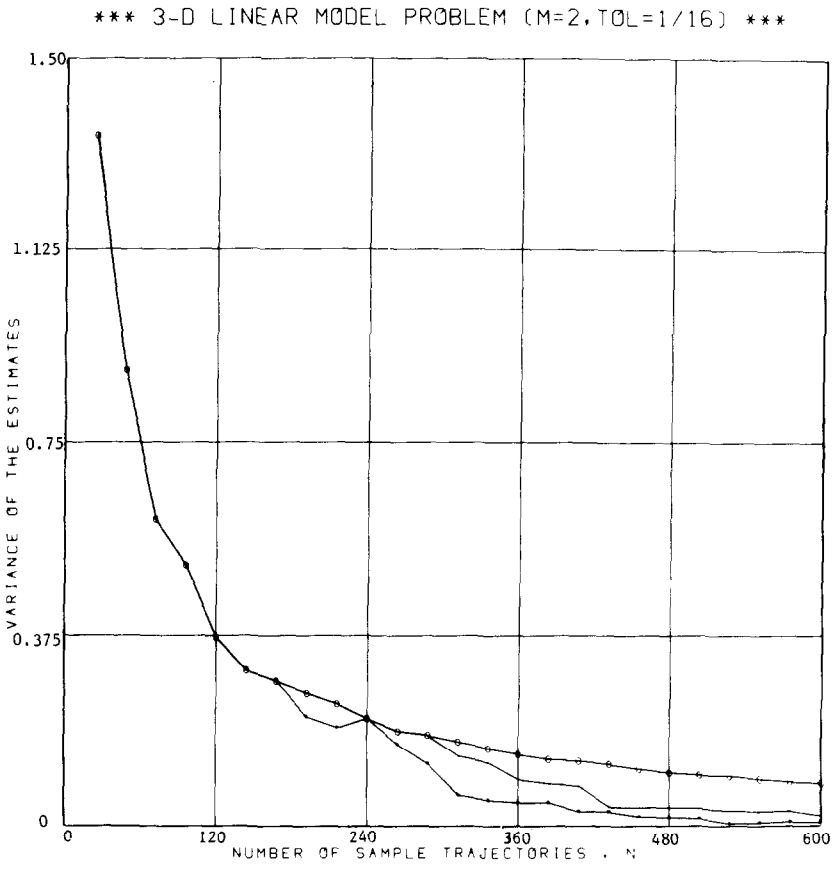

FIG. 6b. Monte Carlo error variances for the three estimates shown in Fig. 6a. Note the resultant variance reductions with the SC estimator for $N > 240$ and with the TSC estimator for $N > 288$. This behavior is typical—the SC estimate yields a variance reduction earlier while the TSC estimate always achieves the smallest asymptotic variance as $N \to \infty$.

For the quadratic functions y_1^2 depicted in Figs. 7a, b, the corresponding evaluations are

$$\hat{y}_1^2 = 4.0576 + 0.9310x_4^2 + 1.8702x_1x_4 + 2.3265x_1x_7 + 1.4350x_1x_{10} + 1.7526x_4x_7 + 1.5772x_4x_{10} + 1.3423x_7x_{10} \quad \text{at} \quad N = 360, \tag{44}$$

$$\hat{y}_1^2 = 4.0152 + 0.8802x_4^2 + 1.1591x_7^2 + 0.6926x_{10}^2 + 1.9179x_1x_4 + 2.0637x_1x_7 + 1.6380x_1x_{10} + 1.8172x_4x_7 + 1.6898x_4x_{10} + 1.3386x_7x_{10} \quad \text{at} \quad N = 480, \tag{45}$$

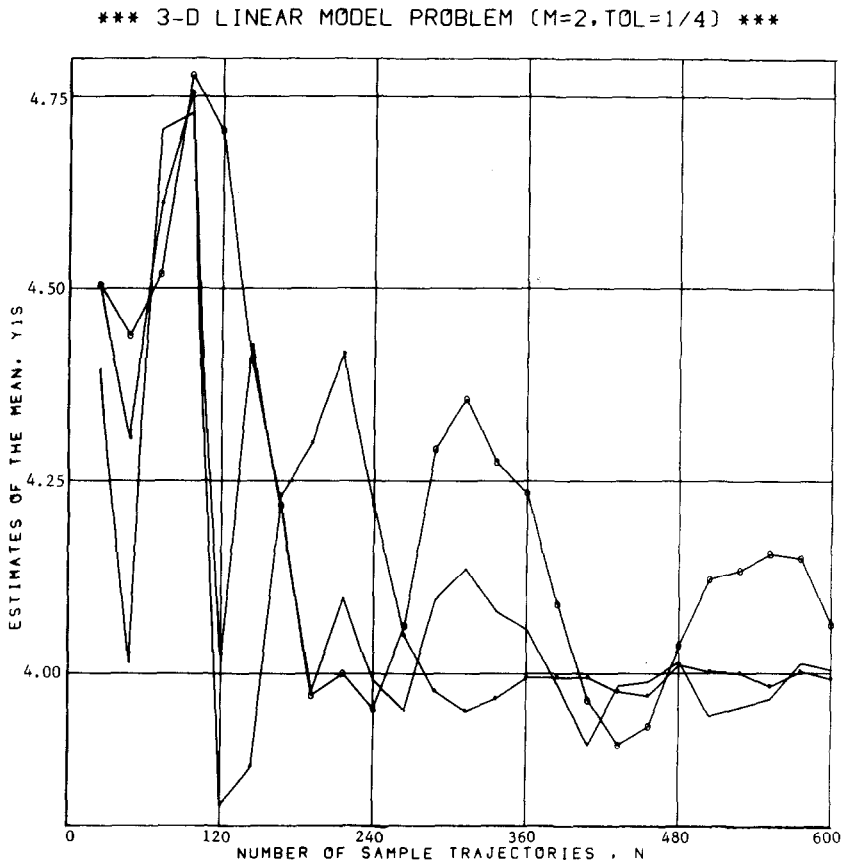

FIG. 7a. Estimates of the mean of y_1^2 as a function of N for the deployment dispersion function $\mathbf{y} = A\mathbf{x} + \boldsymbol{\mu}$. The exact value is $E[y_1^2] = 4.0$. Note, in particular, the superior performance of the SC estimator for $N \geqslant 360$. The complete corrector series here contains a total of 90 terms.

and

$$\hat{y}_1^2 = 4.0041 + 1.2831x_1^2 + 1.0361x_4^2 + 1.1282x_7^2 + 0.9619x_{10}^2 + 2.0237x_1x_4 + 2.1646x_1x_7 + 1.8042x_1x_{10} + 2.0314x_4x_7 + 1.7588x_4x_{10} + 1.4193x_7x_{10} \quad \text{at} \quad N = 600 \tag{46}$$

for the TSC estimator with $m = 2$ and $\text{Tol} = \frac{1}{4}$. Again, the exact form is

$$y_1^2 = (x_1 + x_4 + x_7 + x_{10})^2 = x_1^2 + x_4^2 + x_7^2 + x_{10}^2 + 2[x_1x_4 + x_1x_7 + x_1x_{10} + x_4x_7 + x_4x_{10} + x_7x_{10}].$$

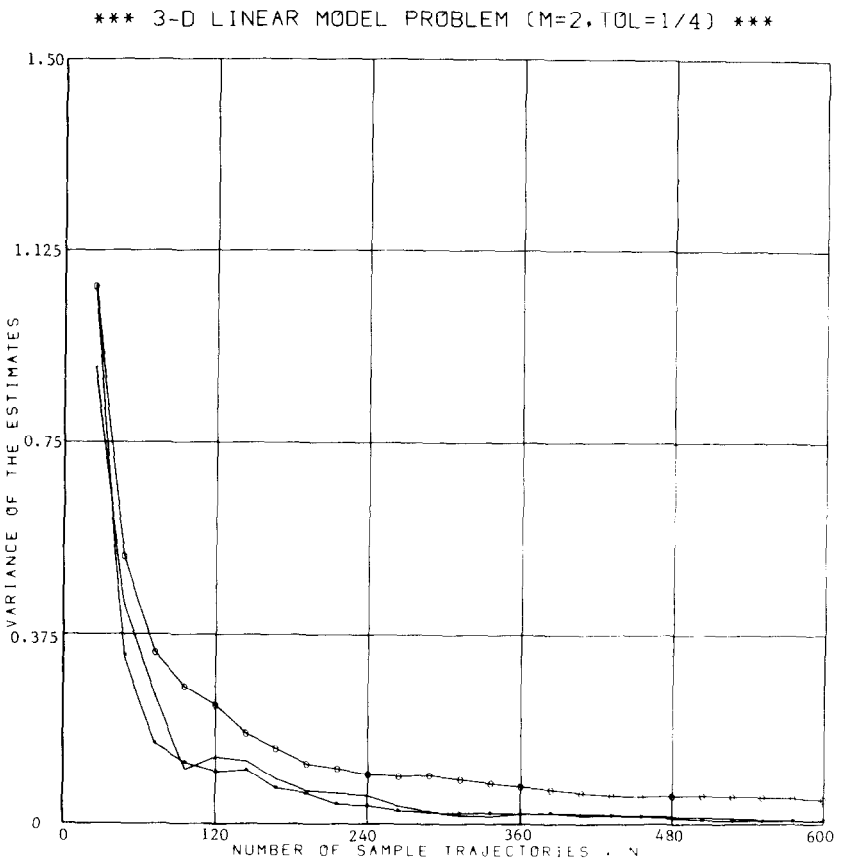

FIG. 7b. Monte Carlo error variances for the three estimates shown in Fig. 7a. Roughly an 8:1 reduction in variance is achieved at $N = 600$.

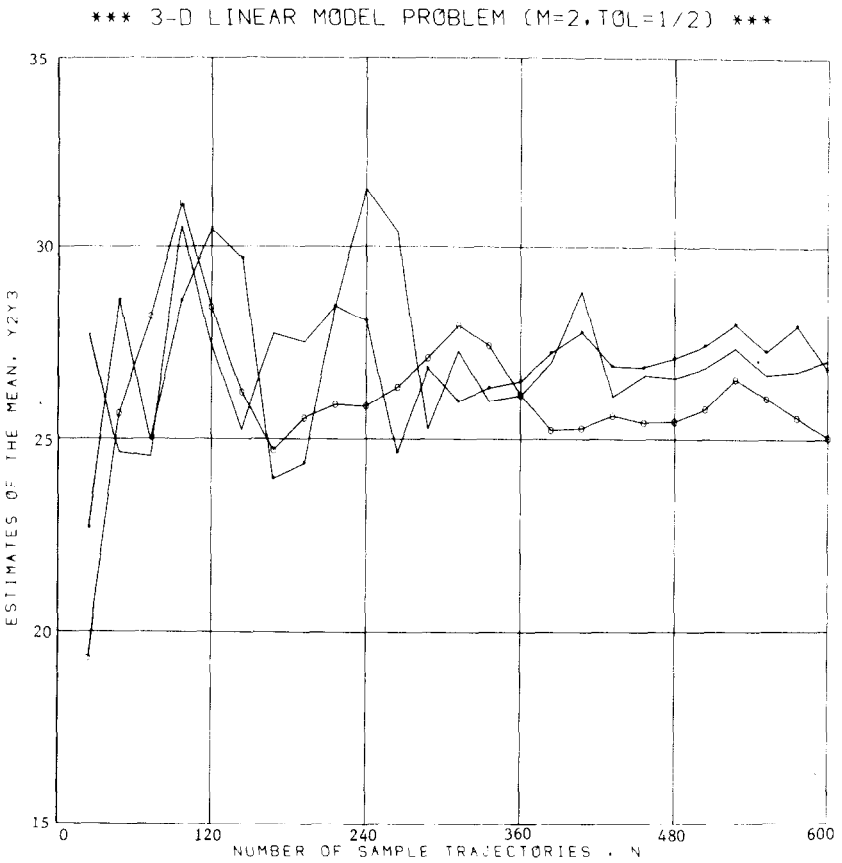

FIG. 8a. Estimates of the mean of $y_2 y_3$ as a function of N for the deployment dispersion function $\mathbf{y} = A\mathbf{x} + \boldsymbol{\mu}$. The exact value is $E[y_2 y_3] = 27.0$.

Finally, it is important to emphasize that, in all cases, these results were obtained automatically by the computer subject only to the preset input quantities m and Tol.

CONCLUSIONS

As shown both in theory and in numerical experiments, the symmetrized estimators described here have been able to furnish valuable reductions in Monte Carlo estimation errors. Furthermore, the adaptive series selection technique has proven to be an essential addition to these advanced Monte Carlo estimators. The adaptive algorithm is based on the fact that the variance reducing (or increasing!) effect of each term in the complete (and generally nonlinear) correction series can be isolated. This important result is obtained by inspection of the exact theoretical expression for

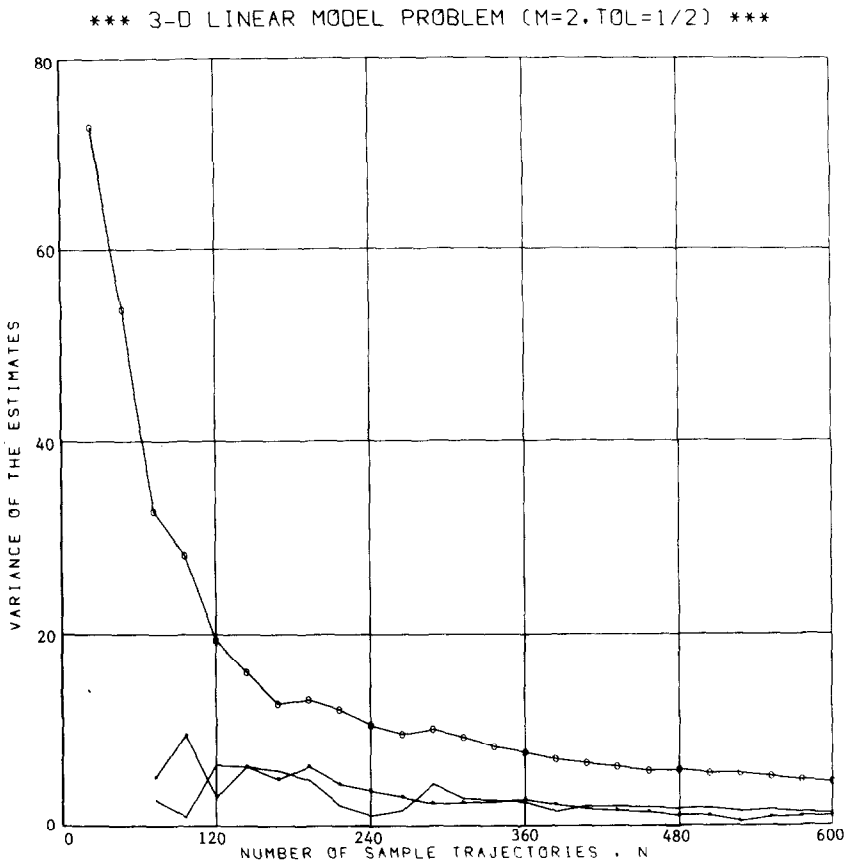

FIG. 8b. Monte Carlo error variances for the three estimates shown in Fig. 8a. Roughly a 4:1 reduction in variance is achieved at $N = 600$.

the estimator variance and leads to the so-called variance reduction discriminant given by Eq. (31).

We consider the use of these orthonormal function space expansions to be a definite advance in Monte Carlo computations since, in general, both variance reduction and system identification is provided. In particular, the further insights obtained from the additional processing of the basic Monte Carlo data should prove, in most cases, to be of considerable importance. Since it is hoped that others might apply these techniques to their problems, the present version of the computer program has been documented [7].

Finally, it should be emphasized that these advanced estimators were developed originally for application to multi-parameter trajectory simulations. In particular, estimates of increased precision were desired for such quantities as range and impact point. A future publication [8] will show the gains that can be achieved when these

adaptive estimators are applied to actual multi-parameter boost and reentry trajectory computations. Presently, we have computational experience with realistic simulations involving 8, 17, 32, 35, and 40 random input parameters.

ACKNOWLEDGMENTS

It is a pleasure to acknowledge Dr. R. J. Dickson, Jr., Dr. P. R. Hempel, Mr. D. L. McGough, T. J. Ross, B. Y. H. Wong, and F. Zele of the Lockheed Missiles and Space Company for their continuing interest and support. Also, we wish to thank Mrs. Betty Charles for her efforts in preparing the original manuscript for publication.

REFERENCES

1. A. J. CHORIN, *J. Comput. Phys.* **8** (1971), 472–482.
2. F. H MALTZ AND D. L. HITZL, *J. Comput. Phys.* **32** (1979), 345–376.
3. F. H. MALTZ AND D. L. HITZL, *in* "Proceedings, Joint Automatic Control Conference, Denver, Colorado, 1979;" also *J. Guidance and Control* **3** (1980), 251–256.
4. J. M. HAMMERSLEY AND D. C. HANDSCOMB, "Monte Carlo Methods," Methuen, London, 1964.
5. J. M. HALTON, *SIAM Rev.* **12** (1970), 1–63.
6. B. Y. H. WONG, "6D/3D Monte Carlo Trajectory Computer Program (MCARLO)," LMSC Technical Memorandum D477772, 1977.
7. F. ZELE AND D. L. HITZL, "Advanced Monte Carlo Software for IAP Applications," LMSC Technical Report D676956, 1979.
8. D. L. HITZL *et al.*, Applications of an adaptive procedure to accelerate Monte Carlo computations, in preparation.